

Investigation of Δ -medium effects using the ${}^4\text{He}(\gamma, \pi^+ n){}^3\text{H}$ and ${}^4\text{He}(\gamma, \pi^+ p)nnn$ reactions

D. Branford,¹ J. F. Arneil,¹ J. A. MacKenzie,¹ K. Föhl,¹ J. Ahrens,² J. R. M. Annand,³ R. Beck,² S. Franczuk,³ P. Grabmayr,⁴ S. J. Hall,³ P. D. Harty,³ T. Hehl,⁴ J. D. Kellie,³ M. Liang,¹ I. J. D. MacGregor,³ J. C. McGeorge,³ A. Natter,⁴ S. Oberkirsch,⁴ R. O. Owens,³ C. J. Y. Powrie,³ D. P. Watts,³ and S. Wunderlich⁴

¹*Department of Physics and Astronomy, University of Edinburgh, Edinburgh EH9 3JZ, Scotland*

²*Institut für Kernphysik, Johannes-Gutenberg Universität, D-55099 Mainz, Germany*

³*Department of Physics and Astronomy, University of Glasgow, Glasgow G12 8QQ, Scotland*

⁴*Physikalisches Institut, Universität Tübingen, D-72076 Tübingen, Germany*

(Received 28 January 2002; published 26 July 2002)

Measurements of the ${}^4\text{He}(\gamma, \pi^+ n){}^3\text{H}$ and ${}^4\text{He}(\gamma, \pi^+ p)nnn$ reactions in quasifree π production kinematic regimes have been performed using unpolarized and linearly polarized tagged photons in conjunction with large solid angle π and n detectors at the MAMI-B accelerator, Mainz. Differential cross sections are presented for photon energies spanning the $\Delta(1232)$ excitation region. These data combined with previously presented results for the ${}^{12}\text{C}(\gamma, \pi^+ n){}^{11}\text{B}$ reaction provide an extensive data set for future investigations of Δ -medium effects in nuclei. The ${}^4\text{He}(\gamma, \pi^+ n){}^3\text{H}$ cross sections are significantly smaller than theoretical predictions based on the free proton amplitude for Δ excitation with a crude correction for final state interactions, and exhibit different trends, which could possibly be a consequence of Δ -medium effects. From a comparison with published ${}^{12}\text{C}(\gamma, \pi^+ p){}^{11}\text{Be}$ data, it is concluded that the ${}^4\text{He}(\gamma, \pi^+ p)nnn$ reaction mechanisms are probably two-step processes, although the possibility that part or all of the cross section arises from interactions with preexisting Δ^{++} particles cannot be ruled out.

DOI: 10.1103/PhysRevC.66.015208

PACS number(s): 25.20.Lj, 13.60.Le, 13.60.Rj

INTRODUCTION

It is well known that in-medium nucleon excitation to the $\Delta(1232)$ resonance state is an important degree of freedom that has to be considered in the descriptions of a wide range of intermediate to high energy nuclear reactions (see, for example, Refs. [1–4]). However, inclusion of Δ excitation in the reaction models is hampered by a lack of experimental evidence for the modifications that are predicted to occur to the free nucleon Δ excitation, propagation, and decay amplitudes in the medium due to interactions with surrounding nucleons (Δ nuclear medium effects). Regarding this point, several authors (e.g., Refs. [5–8]) have concluded on theoretical grounds that sensitive tests of Δ -medium effects may follow from studies of $(\gamma, \pi N)$ reactions in quasifree kinematic regimes.

Models of the $(\gamma, \pi N)$ reactions (e.g., Refs. [7,8]) indicate that a small reduction of $\sim 3\%$ in the Δ mass due to nuclear binding leads to the $N + \gamma \rightarrow \Delta$ excitation cross section close to resonance being reduced by up to a factor of ~ 0.5 . This cross section is also expected [7] to be decreased by an additional few percent due to a predicted increase in the nucleon distortion in the nuclear environment, which will lead to an increase of the ratio of the main $E2$ and $M1$ amplitudes, $R(E2/M1)$. The width of the Δ resonance observed in inclusive photoabsorption measurements exhibits a significant increase thought to be due largely to Fermi motion (e.g., Ref. [9]). However, a reduction in the intrinsic Δ width is expected at low γ energies due to Pauli blocking when the recoiling nucleon has an energy below the Fermi level, and at higher energies, it is anticipated that the intrinsic width will be increased by collision broadening due to the opening up in the medium of the decay mode $\Delta + N \rightarrow N$

+ N (e.g., Refs. [1–4,10]). Clearly, the cumulative effect of such medium modifications could lead to $(\gamma, \pi N)$ reaction cross sections in the nuclear medium exhibiting a different behavior with respect to E_γ and θ_π , and being quite different in magnitude to those observed on free nucleons.

In previous papers, we described the first studies of the ${}^{12}\text{C}(\gamma, \pi^+ n){}^{11}\text{B}$ and ${}^{12}\text{C}(\gamma, \pi^+ p){}^{11}\text{Be}$ reactions made using tagged photons and large solid angle detectors [11–13]. The aim was to make a global search for Δ -medium effects by covering as broad an energy and angular range as possible. Although excellent fits to the shapes of the differential cross sections and n angular distributions were obtained for the ${}^{12}\text{C}(\gamma, \pi^+ n){}^{11}\text{B}$ data using both the calculated results of Refs. [7] and [8], the experimental data were found to be consistently lower than the $M_\Delta = 1232$ MeV calculations as would be expected in the presence of Δ -medium effects. However, it was not possible to quantify the effects unambiguously in terms of a reduction in M_Δ , or any other parameters, due to statistical errors and uncertainties in the final state interaction (FSI) calculations. A more recent measurement of the reaction ${}^{16}\text{O}(\gamma, \pi^- p){}^{15}\text{N}$ at $E_\gamma \approx 300$ MeV, which included polarization asymmetry results, gave no evidence for a large quantifiable modification of the Δ mass, although it is not clear how large a shift is ruled out [14].

In this paper, we describe measurements of the ${}^4\text{He}(\gamma, \pi^+ n){}^3\text{H}$ and ${}^4\text{He}(\gamma, \pi^+ p)nnn$ reactions, which follow on from our previous measurements on ${}^{12}\text{C}$. These measurements were carried out with the aim of providing new high-resolution data, with a higher statistical accuracy than for the C target, against which models of $\Delta(1232)$ nuclear medium effects can, in future, be tested. The new data include photon asymmetries, which provide an alternative indicator of Δ -medium effects, which is insensitive to the treatment of FSI. A ${}^4\text{He}$ target was chosen because the cen-

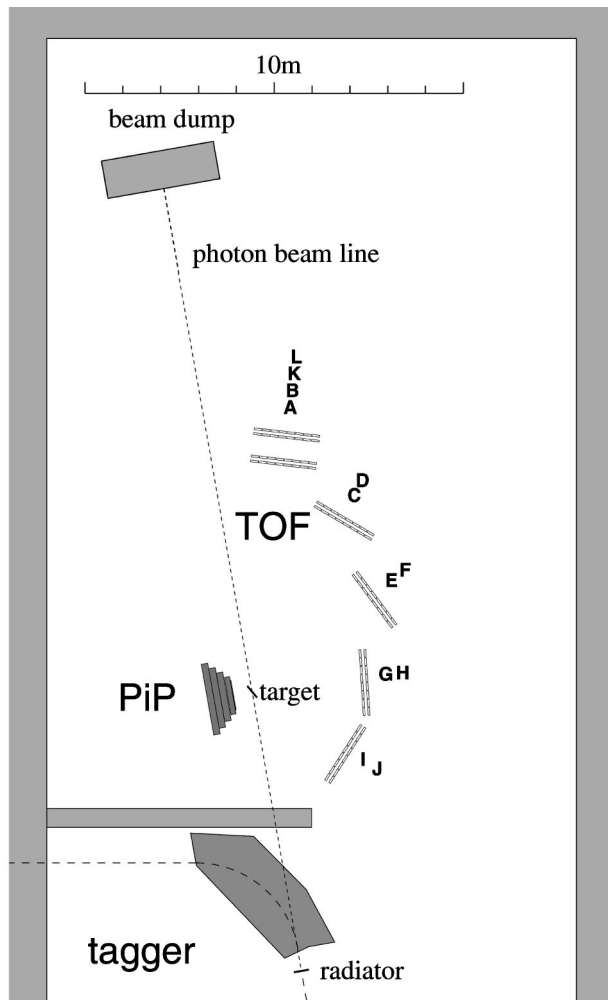


FIG. 1. Experimental arrangement used for the ${}^4\text{He}(\gamma, \pi^+n){}^3\text{H}$ and ${}^4\text{He}(\gamma, \pi^+p)nnn$ measurements.

tral density is higher than that of any other nucleus, from which it follows that larger medium effects are expected. Also, the FSI are expected to be smaller than in the ${}^{12}\text{C}$ study. In addition, since only 1s shell nucleons are involved in the ${}^4\text{He}$ reaction, there is no need to resolve events due to the removal of protons from different shells, which have very different angular distributions, as was the case for the ${}^{12}\text{C}(\gamma, \pi^+n){}^{11}\text{B}$ study [12].

The new experiment included the first detailed investigation of the ${}^4\text{He}(\gamma, \pi^+p)nnn$ reaction, which complements our ${}^{12}\text{C}(\gamma, \pi^+p){}^{11}\text{Be}$ measurement [13]. The results of the ${}^{12}\text{C}(\gamma, \pi^+p){}^{11}\text{Be}$ experiment have recently been interpreted as providing evidence for preexisting Δ^{++} s in ${}^{12}\text{C}$ [15]. The new measurement allows this to be investigated further.

EXPERIMENTAL ARRANGEMENT

Figure 1 shows the experimental arrangement, which was very similar to that used for our previous studies of the ${}^{12}\text{C}(\gamma, \pi^+n){}^{11}\text{B}$ and ${}^{12}\text{C}(\gamma, \pi^+p){}^{11}\text{Be}$ reactions [11–13]. A bremsstrahlung photon beam was produced by a ~ 15 nA beam of electrons from the Mainz microtron (MAMI-B) incident on a 4 μm Ni radiator. The energies of photons in the

range $E_\gamma = 114\text{--}792$ MeV were analyzed using the Glasgow tagging spectrometer [16,17]. The tagged photon resolution and counting rate were typically $\Delta E_\gamma = 2$ MeV and 5×10^7 s^{-1} , respectively. Linearly polarized photons were produced using coherent bremsstrahlung from a diamond radiator [18]. Two runs were made with the diamond orientated such that the upper edge of the coherent peak of interest occurred at energies of $E_\gamma \sim 280$ and ~ 360 MeV, respectively. The direction of the polarization was rotated at 20 min intervals between vertical and horizontal planes.

The photon beam was collimated to a diameter of ~ 18 mm and ~ 11 mm at the target for the unpolarized and polarized beam measurements, respectively. For the ${}^4\text{He}(\gamma, \pi^+n){}^3\text{H}$ and ${}^4\text{He}(\gamma, \pi^+p)nnn$ measurements, the target was a Kapton cell of 3 cm diameter and 8 cm length containing liquid ${}^4\text{He}$. This cell was gravity fed by a reservoir of liquid ${}^4\text{He}$, the whole system being housed in an evacuated cryostat that included additional liquid N_2 cooling [19]. The time between reservoir refills was typically 12 h. Calibration runs were made with either a 0.839 g cm^{-2} C or 0.915 g cm^{-2} CH_2 target inclined at an angle of 20° with respect to the beam direction. The fraction of tagged incoherent bremsstrahlung photons passing through the collimator, the tagging efficiency, was measured several times and remained stable at $55 \pm 1\%$. The tagging efficiency for the diamond radiator varies significantly with photon energy, but, at a given E_γ , it is the same for the two polarization directions and therefore cancels in the photon asymmetry measurement.

The energies and angles of particles produced in the target were measured by two large solid-angle detection systems. On one side of the beam, a plastic scintillator hodoscope (PiP) [20] was used to detect charged particles in the polar angle range $\theta = 50^\circ\text{--}130^\circ$ and azimuthal range $\phi = -24^\circ$ to 24° . Events corresponding to the detection of a π^+ were selected using ΔE versus E information and demanding that an afterpulse from the decay $\mu \rightarrow \beta + 2\nu$ occurred within 6 μs [12]. A time of flight detector array (TOF), placed on the opposite side of the beam, was used to detect neutrons and protons. This detector [21] consisted of 6 stands each containing 16 vertically mounted scintillators of dimension $3000 \times 200 \times 50$ mm^3 in two ranks of 8 (see Fig. 1) and covered the polar angle range $\theta = 10^\circ\text{--}150^\circ$. The range of azimuthal angles ϕ covered by each element depended on the distance from the target, which was between 3 and 7 m. Surrounding the target at a radius of 11 cm was a ring of thin ΔE scintillator detectors, which had a dual purpose. Used in coincidence with PiP, they produced a trigger pulse for each detected charged particle. On the TOF side, the presence or absence of a signal in the appropriate element of this ring and in a second half ring of detectors at 30 cm radius indicated a charged or neutral particle, respectively. The analogue to digital converter (ADC) and time to digital converter (TDC) information was read out using the so-called ACQU data acquisition system [22].

DETECTOR CALIBRATION AND DATA ANALYSIS

As explained in our previous paper [12], the main innovation of our quasifree $(\gamma, \pi N)$ measurements is the use of a

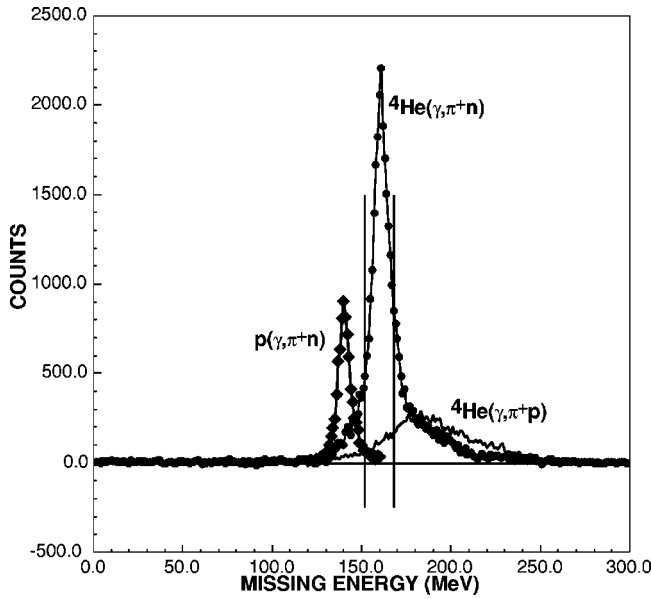


FIG. 2. Missing energy spectra for the $p(\gamma, \pi^+n)$, ${}^4\text{He}(\gamma, \pi^+n)$, and ${}^4\text{He}(\gamma, \pi^+p)$ reactions.

plastic scintillator hodoscope to detect pions rather than a magnetic spectrometer, which is more conventional. This choice was made because magnetic spectrometers with sufficiently high resolution have too small an acceptance to allow a broad range measurement of the type described here. Since scintillator hodoscopes had not been used previously to detect pions with such high energies, the analysis techniques were fully described in Ref. [12], to which the reader is referred for details of the detector calibration and data analysis.

RESULTS AND DISCUSSION

The missing energy distributions

The missing energy for each measured $(\gamma, \pi N)$ event was obtained using the equation

$$E_m = E_\gamma - E_\pi - E_N - E_{recoil} = E_x - Q, \quad (1)$$

where E_γ is the energy of the tagged photon, E_π is the kinetic energy of the π , E_N is the kinetic energy of the emitted nucleon, and E_{recoil} is the kinetic energy of the recoiling system of mass $(A-1)$ determined using momentum conservation. E_x and Q are the excitation energy associated with the $(A-1)$ system and the Q value for the reaction leading to the ground state, respectively. The $p(\gamma, \pi^+n)$ data were obtained using the CH_2 target; separation of the $p(\gamma, \pi^+n)$ data from that of the ${}^{12}\text{C}(\gamma, \pi^+n){}^{11}\text{B}$ reaction being achieved by demanding for each event that E_n and θ_n occurred close to the values calculated from E_γ and θ_π using the $p(\gamma, \pi^+n)$ reaction kinematics.

The measured missing energy distributions are shown in Fig. 2. The $p(\gamma, \pi^+n)$ reaction spectrum has a single peak with a centroid at $E_m = 140.5 \pm 0.2$ MeV (statistical error only), which is consistent with the reaction Q value of 140.8 MeV and the ± 1 MeV estimated systematic error in the

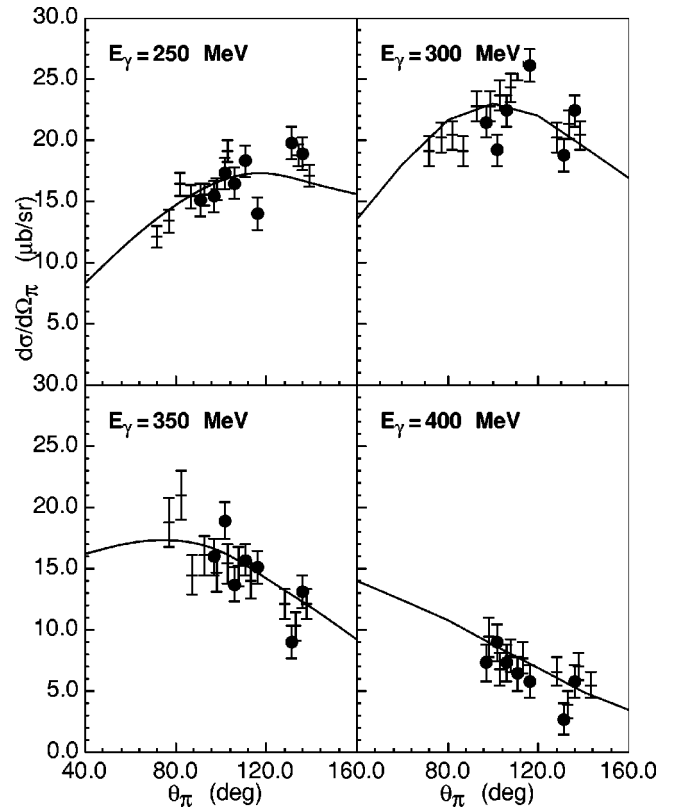


FIG. 3. Differential cross sections for the $p(\gamma, \pi^+n)$ reaction in the center-of-mass system. The curves were calculated using the theory of Blomqvist and Laget [25], which gives a good description of previous experimental data [26]. The data points from the present (solid circles) and previous experiment (horizontal crosses) [12,23] have been increased in magnitude by a factor of 1.16 and 1.20, respectively.

missing energy determinations. The full width at half maximum (FWHM) resolution was $\Delta E_m = 8.0$ MeV, which agrees well with an estimate obtained by adding in quadrature the resolutions $\Delta E_\gamma = 2$ MeV, $\Delta E_\pi = 7$ MeV, and $\Delta E_n = 3.0$ MeV associated with the tagging system, PiP, and TOF, respectively [23,24].

As described previously [11,12,23], $p(\gamma, \pi^+n)$ cross sections were obtained by integrating over the kinematically allowed E_π , θ_n , and ϕ_n ranges appropriate to each selected pair of E_γ and θ_π bins. These cross sections are compared in Fig. 3 to previous results [11,12,23], and calculations using the expressions of Blomqvist and Laget [25], which reproduce the previously measured cross sections (e.g., Ref. [26]) for this reaction. For this comparison, the calculated cross sections were averaged over the appropriate E_γ bins and detector angles. An overall normalization factor of 1.16 is required to bring the present $p(\gamma, \pi^+n)$ results in agreement with the calculations, which compares favorably with 1.20 used in Refs. [11,12,23]. Since the factor of 1.16 is consistent with the total systematic error of 20%, estimated from the uncertainties in target thickness, tagging efficiency, detector efficiencies, and solid angles, the ${}^4\text{He}(\gamma, \pi^+n)$ data were normalized by the same factor of 1.16. The systematic error of the normalized ${}^4\text{He}(\gamma, \pi^+n)$ data is obtained by combin-

ing the statistical errors of the present $p(\gamma, \pi^+n)$ data with the systematic errors of about $\pm 4\%$ for the previous data [26]. The resulting systematic error, $\pm 10\%$, is significantly reduced compared to the systematic error of the ${}^4\text{He}(\gamma, \pi^+n)$ measurements taken alone.

The large peak in the missing energy spectrum for the ${}^4\text{He}(\gamma, \pi^+n)$ reaction shown in Fig. 2 occurs at $E_m = 158.5 \pm 0.1$ MeV (statistical error only) and has a FWHM of $\Delta E_m \sim 10.5$ MeV. The fact that the peak from the ${}^4\text{He}(\gamma, \pi^+n)$ data occurs close to the threshold Q value (160.2 MeV) and has a width that is not appreciably greater than 8.0 MeV suggests that the observed events arose predominantly from the removal of a single proton leaving the residual ${}^3\text{H}$ nucleus intact and involved relatively small FSI. To select events which are almost exclusively of this nature, an $E_m = 152\text{--}168$ MeV cut on the data was made as indicated in Fig. 2. The fraction of quasifree events excluded by this cut was corrected for each of the four E_γ bins by considering the tail on the low E_m side of the peak. The tail at higher E_m is assumed to be due to nonquasifree processes and FSI, which will generally result in the breakup of the residual ${}^3\text{H}$. It is also assumed that only a small number of counts from events of the types found in this tail will be present in the $E_m = 152\text{--}168$ MeV region, since the thresholds for ${}^3\text{H}$ breakup to ${}^2\text{H}+n$ and $2n+p$ occur at $E_m = 166.5$ and 168.7 MeV, respectively.

Differential cross sections

Figures 4 and 5, which were obtained using the bins listed in Table I, show the θ_n dependence of the ${}^4\text{He}(\gamma, \pi^+n){}^3\text{H}$ cross section in the energy range $E_\gamma = 240\text{--}400$ MeV for four θ_π bins. Figure 6 shows the E_π dependence of the cross section at the average π angles $\theta_\pi = 67^\circ$ and 112° . For these data, the θ_π and θ_n bins were 10° and 15° wide, respectively, and the θ_n bins were centered in each case around the θ_n angle at which the yield of neutrons from quasifree π^+ production is expected to be greatest.

The dashed curves shown in Figs. 4–6 are from plane wave impulse approximation (PWIA) calculations of ${}^4\text{He}(\gamma, \pi^+n){}^3\text{H}$ cross sections produced for this publication [27] using the model of Ref. [7]. For these calculations, the initial nucleon bound state was represented by a harmonic oscillator wave function, which was considered adequate for the predominantly low initial nucleon momenta involved in quasifree π production. The π photoproduction process was described using the full Blomqvist-Laget phenomenological operator [25,28,29]. The results are averaged over the appropriate detector acceptances and multiplied by a spectroscopic factor of $S=0.8$ [30]. Inclusion of FSI into the calculations using the distorted wave impulse approximation (DWIA) code of Ref. [7], which uses the optical model to determine the distortions in the outgoing waves, was not considered appropriate to the very light nucleus ${}^4\text{He}$. Therefore, in the absence of more exact calculations, we have made an initial investigation using a crude estimate of the FSI. Although this cannot be used to provide a quantitative measure of Δ -medium effects, it was anticipated that it would highlight the more interesting features of the experimental data.

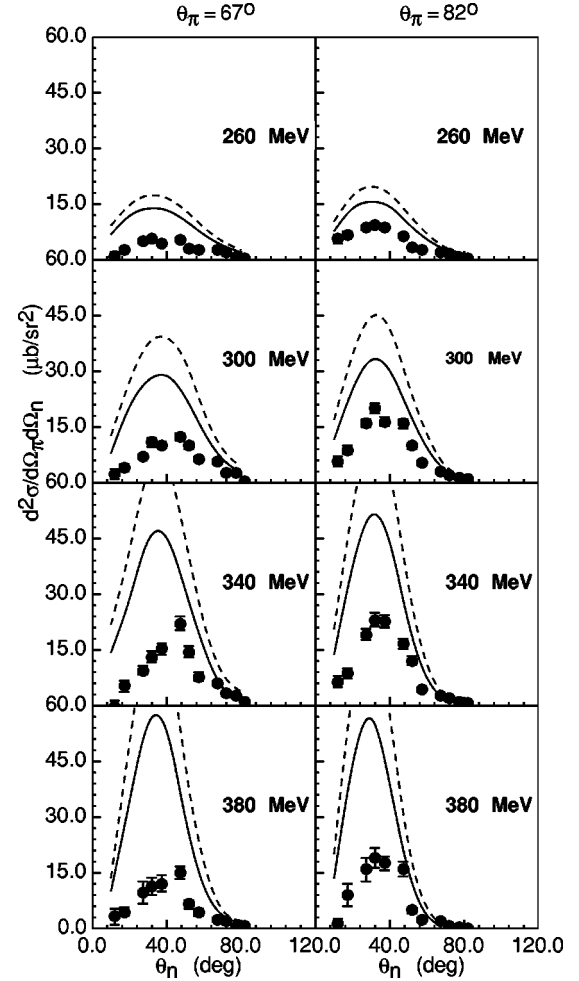
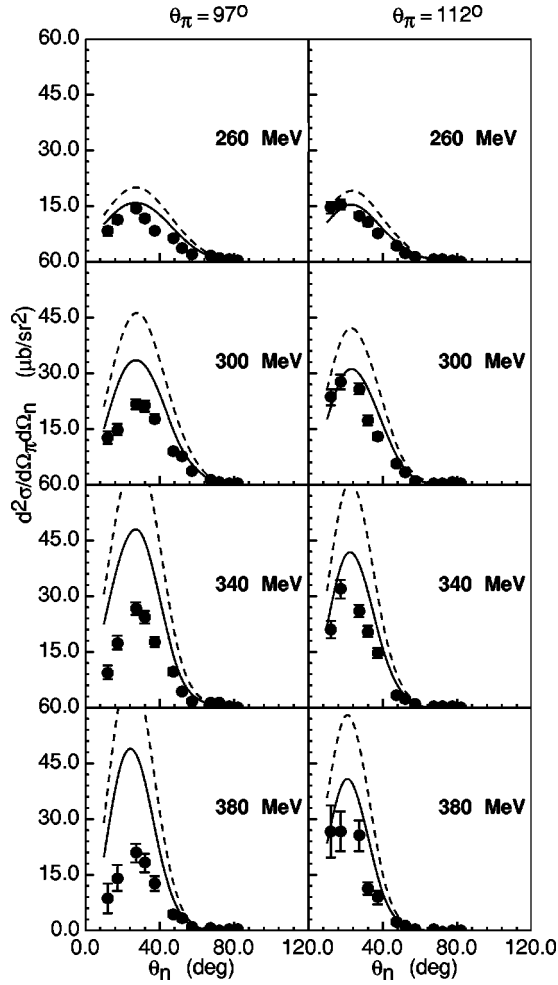


FIG. 4. Differential cross sections for the ${}^4\text{He}(\gamma, \pi^+n){}^3\text{H}$ reaction versus n laboratory angle obtained at average π detection angles of $\theta_\pi = 67^\circ$ and 82° , and average photon energies $E_\gamma = 260, 300, 340,$ and 380 MeV. The $E_\gamma, \theta_\pi, \phi_\pi, \theta_n,$ and ϕ_n bins are listed in Table I. The results are integrated over the E_π and E_n acceptance of the detectors. The theory curves are from PWIA (dashed) calculations and DWIA* (solid) estimates obtained for $M_\Delta = 1232$ MeV.

In our simple approach, we estimated the effects of the FSI for the ${}^4\text{He}(\gamma, \pi^+n){}^3\text{H}$ reaction based on the PWIA and DWIA calculations for the ${}^{12}\text{C}(\gamma, \pi^+n){}^{11}\text{B}$ experiment [12]. Assuming that the reduction in the exclusive $(\gamma, \pi N)$ cross section due to FSI can be approximated by a factor $\exp(-R/r_0)$, where R is the target radius and the same absorption length r_0 applies to both nuclei, then the effective DWIA* cross section for ${}^4\text{He}$ is given by

$${}^4\text{He}(\text{DWIA}^*) = {}^4\text{He}(\text{PWIA}) \times \frac{{}^{12}\text{C}(\text{DWIA}) \exp(-R_{\text{He}}/r_0)}{{}^{12}\text{C}(\text{PWIA}) \exp(-R_{\text{C}}/r_0)}, \quad (2)$$

where R_{He} and R_{C} are the ${}^4\text{He}$ and ${}^{12}\text{C}$ radii, respectively. Average values for r_0 were obtained from the ${}^{12}\text{C}(\gamma, \pi^+n){}^{11}\text{B}$ calculations at each of the four average photon energies $E_\gamma = 260, 300, 340,$ and 380 MeV, and used to determine ${}^4\text{He}(\text{DWIA}^*)$ results at each E_γ using the ap-

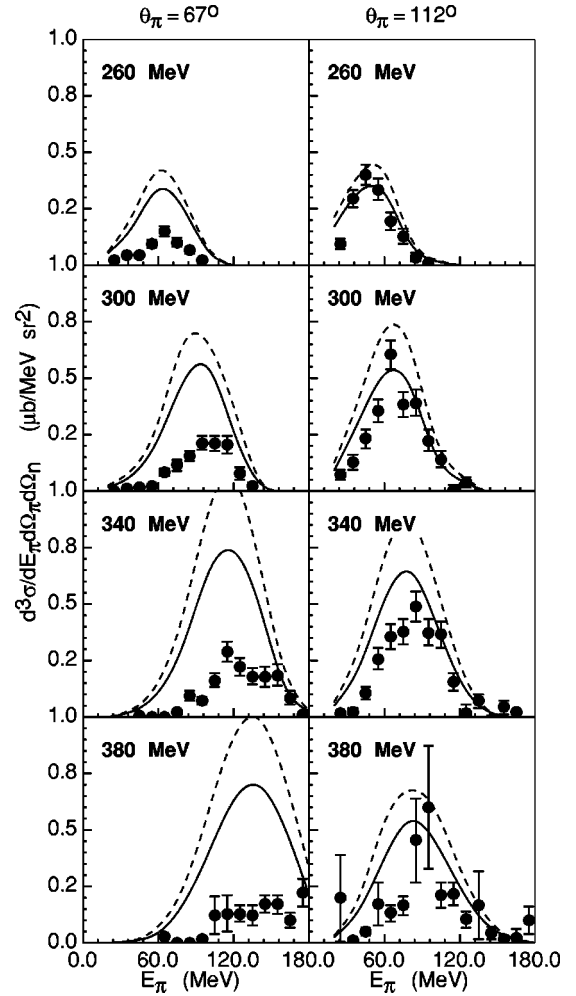

 FIG. 5. As for Fig. 4 for $\theta_\pi = 97^\circ$ and 112° .

appropriate r_0 . These results are shown as solid curves in Figs. 4–6. Typically, application of Eq. (2) results in the ${}^4\text{He}(\text{PWIA})$ cross section being reduced by $\sim 25\%$, which can be considered a rough estimate of the amount lost due to FSI. This is approximately half of the FSI losses determined from the DWIA calculations used in considering the ${}^{12}\text{C}(\gamma, \pi^+ n){}^{11}\text{B}$ measurement [12].

It is clear from Figs. 4–6 that the shapes of the n angular distributions and π kinetic energy spectra are well described by the PWIA and DWIA* calculations. Since these shapes are dominated by the wave function used to describe the proton in the ${}^4\text{He}$ ground state, it can be assumed that use of

 TABLE I. The binning regions used in extracting the ${}^4\text{He}(\gamma, \pi^+ n){}^3\text{H}$ and ${}^4\text{He}(\gamma, \pi^+ p)nnn$ cross sections.

Quantity	Range	Bin size	No. of bins
E_γ	240–400 MeV	40 MeV	4
E_π	20–180 MeV	10 MeV	16
θ_π	60–120°	15°	4
ϕ_π	(–15)–15°	30°	1
θ_N	10–150°	5°	28
$\phi_N - \phi_\pi$	170–190°	20°	1


 FIG. 6. Differential cross sections for the ${}^4\text{He}(\gamma, \pi^+ n){}^3\text{H}$ reaction versus π^+ kinetic energy. The θ_π and θ_n bins are 10° and 15° wide, respectively. The ϕ_π and ϕ_n bins are listed in Table I. The results are integrated over the E_n detector acceptance. The theory curves are from PWIA (dashed) calculations and DWIA* (solid) estimates obtained using $M_\Delta = 1232$ MeV.

a harmonic oscillator potential is adequate to describe the data. This conclusion differs from that arrived at by Hicks *et al.* [14] following their study of the ${}^{16}\text{O}(\gamma, \pi^- p){}^{15}\text{N}$ reaction at $E_\gamma \approx 300$ MeV. At the largest proton angle measured, $\theta_p = 75^\circ$, the experimental differential cross section versus θ_π is flatter than the theoretical curve, from which it was concluded that the use of a harmonic oscillator potential is inadequate in some kinematics. We consider it more likely, however, that the differences arise because the experimental method used by Hicks *et al.* did not differentiate between the detection of π^- and π^+ particles, and had very poor missing energy resolution, mainly due to the nuclear explosions that occur at the end of each π^- track. Under these circumstances, it would have been very difficult to estimate accurately the relative contributions to the data from $1p$ and $1s$ shell nucleons, the effects of contamination by the ${}^{16}\text{O}(\gamma, \pi^+ p){}^{15}\text{C}$ reaction, detector thresholds, reactions on nucleon pairs, multistep reactions, etc.

Figures 4–6 also show that the experimental data fall sig-

nificantly below the DWIA* results, particularly for the more forward θ_π angles. These results are similar to those observed in our study of the $^{12}\text{C}(\gamma, \pi^+ n)^{11}\text{B}$ reaction [12], which also agreed in shape with the PWIA and DWIA calculations but fell consistently below both. Although again our ^{12}C results differ from the $^{16}\text{O}(\gamma, \pi^- p)^{15}\text{N}$ measurement [14], where agreement in magnitude was found, a direct comparison is not possible since as pointed out in Ref. [14] separation of the contributions from different shells in the ^{16}O experiment was not achieved. We consider it most likely, however, that the differences are a consequence of the problems with the $^{16}\text{O}(\gamma, \pi^- p)^{15}\text{N}$ measurement presented above.

In considering Figs. 4–6 further, we note that differences occur between the experimental cross sections and the DWIA* results at almost all E_γ and θ_π angles. To obtain a better impression of the trends with energy and π emission angles, we determined the θ_π dependence of the $^4\text{He}(\gamma, \pi^+ n)^3\text{H}$ cross section at the average energies $E_\gamma = 260, 300, 340,$ and 380 MeV by integrating the cross sections shown in Figs. 4 and 5 over θ_n . These results are shown in Fig. 7. The data points are presented with $\pm 10\%$ systematic error bars. Figure 8 shows, for comparison, the corresponding data for the $^{12}\text{C}(\gamma, \pi^+ n)^{11}\text{B}$ reaction at the same average E_γ energies obtained from our earlier study [12].

From Figs. 7 and 8, it is evident that the data points lie considerably below the DWIA* results in the region of the $\Delta(1232)$ resonance peak, which is where the Δ -medium effects are expected to be the largest. However, there are even larger relative differences in the more forward θ_π , lower energy $^4\text{He}(\gamma, \pi^+ n)^3\text{H}$ data, where the Born terms are more important. These results suggest that the in-medium quasifree pion production cross sections may vary with E_γ and θ_π quite differently compared to those for free nucleons and hence that medium effects may possibly be present. However, definite conclusions cannot be reached until a proper theoretical calculation including FSI is carried out. Regarding such calculations, it should be noted that the interpretation of our $^4\text{He}(\gamma, \pi^+ n)^3\text{H}$ and $^{12}\text{C}(\gamma, \pi^+ n)^{11}\text{B}$ measurements will require the development of a code that will allow the effects associated with each model parameter to be investigated efficiently over a large range of energies and angles. In particular, it might be useful to investigate varying Γ_Δ and the ratio $R(E2/M1)$, and perhaps even consider allowing Γ_Δ to vary as a function of E_γ to take into account the effects of Pauli blocking at low E_γ and the opening up of the $N + \Delta \rightarrow N + N$ decay channel with increasing E_γ . Clearly, a proper treatment of the FSI for the $^4\text{He}(\gamma, \pi^+ n)^3\text{H}$ data will also be necessary. It is hoped that the large increase in the available data on quasifree π production provided by this work and our previous paper [12] will stimulate further theoretical interest in $\Delta(1232)$ -medium effects leading to the development of a versatile computer code that in the future will provide a more quantitative understanding of the phenomenon.

Photon asymmetry

Photon asymmetries were determined at average photon energies $E_\gamma = 258$ and 358 MeV using the equation

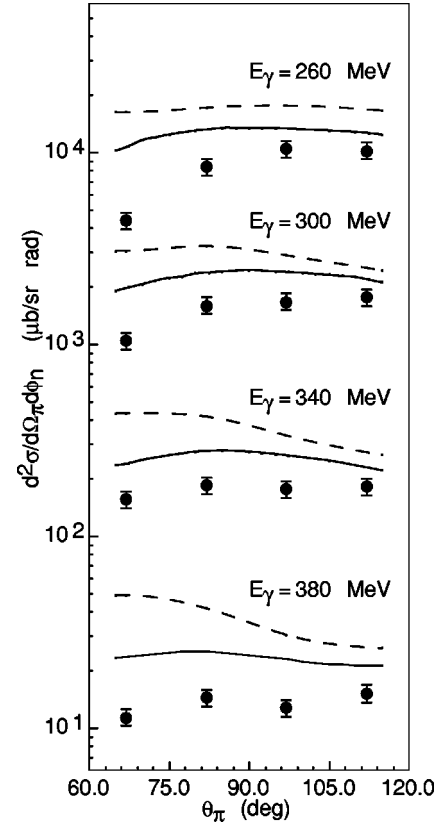


FIG. 7. Differential cross sections for the $^4\text{He}(\gamma, \pi^+ n)^3\text{H}$ reaction versus θ_π at the indicated average photon energies. The solid circles show the measured cross sections integrated over the E_n , E_π , and θ_n acceptances of the detectors. The E_γ , θ_π , ϕ_π , and ϕ_n bins are listed in Table I. The error bars indicate systematic errors of $\pm 10\%$. The dashed and solid lines show PWIA cross sections before and after the crude correction for FSI, respectively. The cross sections at 340, 300, and 260 MeV are multiplied by factors of 10, 100, and 1000, respectively.

$$\Sigma = \frac{1}{P_\gamma} \frac{\sigma_\perp - \sigma_\parallel}{\sigma_\perp + \sigma_\parallel}, \quad (3)$$

where P_γ is the linear polarization of the photon beam, and σ_\perp and σ_\parallel are the cross sections with the polarization vertical and horizontal, i.e. perpendicular and parallel to the reaction plane, respectively. The beam polarization P_γ was determined by performing a Monte Carlo simulation as described in Ref. [31]. This simulation gave the relative intensity, as a function of E_γ , of the coherent and incoherent parts of the bremsstrahlung produced by the diamond, thus enabling the degree of polarization to be determined for the range of tagged photons used in the measurement. The calculation gave average polarizations of 0.50 and 0.40 in the regions $E_\gamma = 268 \pm 20$ and $E_\gamma = 338 \pm 20$, respectively. This procedure has been checked [32] by studying the coherent $^4\text{He}(\gamma, \pi^0)^4\text{He}$ reaction in which the linear polarization of the photon beam is completely transferred to the azimuthal asymmetry of the emitted π^0 mesons since ^4He and the π^0 both have zero spin.

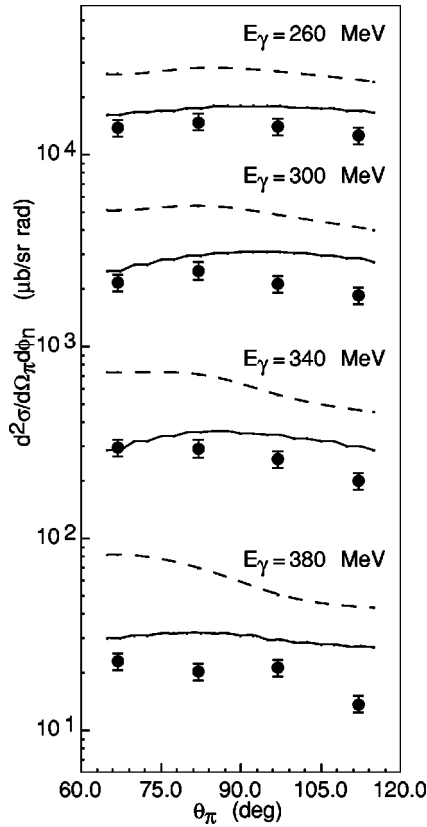


FIG. 8. Differential cross sections for the $^{12}\text{C}(\gamma, \pi^+n)^{11}\text{B}$ reaction versus θ_π at the indicated photon energies obtained from [12]. The results shown as solid circles are integrated over the E_n , E_π , and θ_n detector acceptances. The E_γ , θ_π , ϕ_π , and ϕ_n bins are as listed in Table I. The error bars indicate the systematic errors of $\pm 10\%$. The dashed and solid lines are PWIA and DWIA results, respectively. The cross sections at 340, 300, and 260 MeV are multiplied by factors of 10, 100, and 1000, respectively.

Figure 9 shows the asymmetry results obtained for the $p(\gamma, \pi^+n)$ measurement compared to a curve based on fits to previous Mainz measurements [33]. The curve is corrected for detector acceptances. Although the statistical accuracy is not high, the agreement is reasonable.

Figure 10 shows the results obtained for the $^4\text{He}(\gamma, \pi^+n)^3\text{H}$ reaction at the two E_γ settings, which are below and close to those giving the maximum cross sections for Δ excitation, respectively. Although again the statistical accuracy is not high, it is clear that the asymmetries observed for protons in the medium have the same sign and are comparable in magnitude to the free proton values.

Since the asymmetry calculations are relatively insensitive to FSI, they provide a sensitive probe for medium effects. To make a quantitative assessment, the weighted average of the ratio $R = \sum_i W_i [(\Sigma_D)_i / (\Sigma_T)_i] / \sum_i W_i$ was determined from the data of Fig. 10, where W_i , $(\Sigma_D)_i$, and $(\Sigma_T)_i$ are the statistical weights, experimental asymmetries, and theoretical asymmetries, respectively. Although the result $R = 0.86 \pm 0.09$, is not inconsistent with $R = 1.0$, it is interesting to note that a more accurate measurement for the $^{16}\text{O}(\gamma, \pi^-p)^{15}\text{N}$ reaction [14], which is related by isospin symmetry arguments, gave experimental photon asymmetries

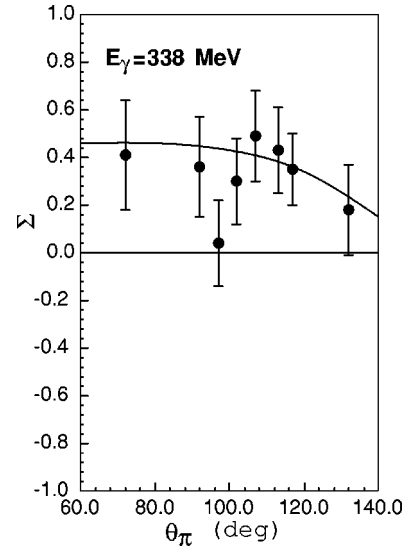


FIG. 9. Measured photon asymmetries Σ versus θ_π for the $p(\gamma, \pi^+n)$ reaction at average $E_\gamma = 338$ MeV. The experimental binning is as for Fig. 3. The solid curve is based on fits to previous measurements made at Mainz [33].

that are less than 1.0. Clearly, in view of this result, it would be worthwhile to obtain more accurate photon asymmetries for the $^4\text{He}(\gamma, \pi^+n)^3\text{H}$ reaction.

The $^4\text{He}(\gamma, \pi^+p)nnn$ reaction

Figures 11 and 12 show differential cross sections obtained for the $^4\text{He}(\gamma, \pi^+p)nnn$ reaction. For those data shown in Fig. 12, the θ_π and θ_p bins were 10° and 15° wide, respectively. The θ_p bins were identical to the θ_n used to produce Fig. 6 and covered the angles at which the yield of coincident protons was the greatest. Although the cross sections are considerably smaller than those measured for the $^4\text{He}(\gamma, \pi^+n)^3\text{H}$ reaction, it was possible to obtain good statistical data at mean photon energies $E_\gamma = 300$ and 340 MeV, due mainly to the fact that the efficiency of individual TOF bars for detecting incident protons is $\sim 100\%$ compared to $\sim 5\%$ for neutrons. At higher E_γ , the results had poor statistical accuracy, and below $E_\gamma = 300$ MeV, the proton energies were below the TOF thresholds due to energy loss along the flight paths.

As the $^4\text{He}(\gamma, \pi^+p)nnn$ cross sections are considerably smaller than those for other reactions, any misidentifications of the particles involved could lead to significant errors. The most likely contamination of the data arises from (γ, π^-p) events in which the π^- particles were misidentified as π^+ particles. Since π^+ particles were identified by observing afterpulses from the $\mu^+ \rightarrow e^+ + 2\nu$ decays and the energy loss in each detector layer was scrutinized to minimize the effects of π -nuclear interactions in the detector, only the 2% of π^- particles that decayed in flight towards the end of their tracks are likely to have been misidentified as π^+ particles. Combining this number with the $^4\text{He}(\gamma, \pi^+p)nnn$ sections, which are $\sim 10\%$ of those for $^4\text{He}(\gamma, \pi^-p)^3\text{H}$ [assumed equal to $^4\text{He}(\gamma, \pi^+n)^3\text{H}$], we estimate that the contribution to the $^4\text{He}(\gamma, \pi^+p)nnn$ cross sections presented here due to

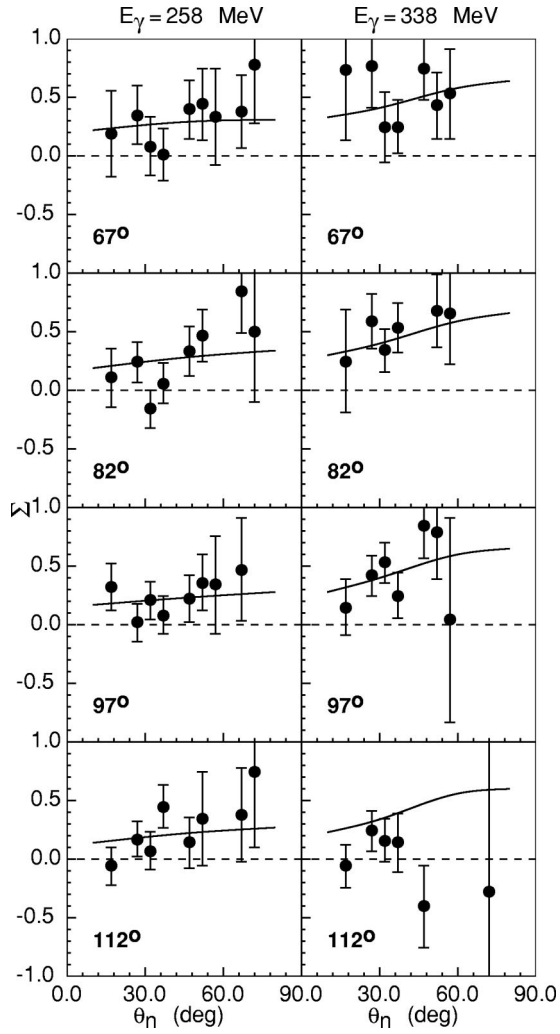


FIG. 10. Measured photon asymmetries Σ versus θ_π for the ${}^4\text{He}(\gamma, \pi^+n){}^3\text{H}$ reaction at average $E_\gamma = 258$ and 338 MeV and the indicated mean θ_π . The results are for all coincident particles detected within the E_n , E_π , and θ_n acceptances of the detectors. The E_γ , θ_π , ϕ_π , and ϕ_n bins are listed in Table I. The solid curves are PWIA calculations obtained using the LWB model and averaged over the detector acceptances.

misidentified π^- particles is $\leq 20\%$. Other systematic errors are estimated to lead to an additional uncertainty of $\pm 15\%$ in the absolute cross sections.

From Fig. 2, it is evident that the missing energy spectrum for the ${}^4\text{He}(\gamma, \pi^+p)nnn$ reaction is broader than that for the ${}^4\text{He}(\gamma, \pi^+n){}^3\text{H}$ reaction and peaks at a higher energy. This is undoubtedly a consequence of the fact that the residual system associated with the ${}^4\text{He}(\gamma, \pi^+p)nnn$ reaction is unbound; the reaction thus proceeds in all cases to a continuum of unbound states. In view of this, it comes as a surprise that the p angular distributions as shown in Fig. 11 are similar to the n distributions obtained in the ${}^4\text{He}(\gamma, \pi^+n){}^3\text{H}$ reaction (Figs. 4 and 5), and the π energy distributions shown in Fig. 12 are similar in shape to those shown in Fig. 6.

The above behavior closely resembles that of the ${}^{12}\text{C}(\gamma, \pi^+n){}^{11}\text{B}$ and ${}^{12}\text{C}(\gamma, \pi^+p){}^{11}\text{Be}$ reactions [13]. The conclusion reached in Ref. [13] was that the (γ, π^+p) events

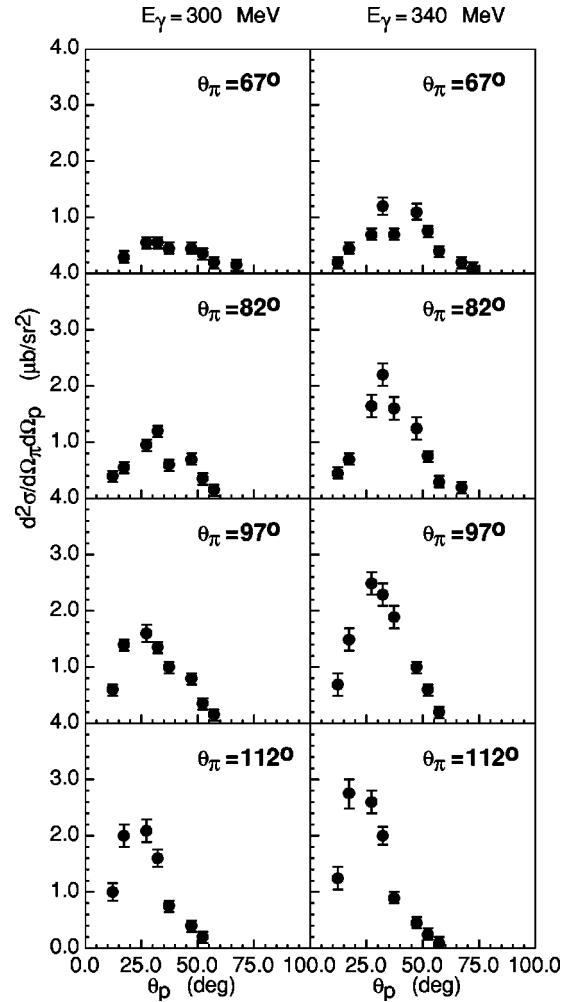


FIG. 11. Differential cross sections for the ${}^4\text{He}(\gamma, \pi^+p)nnn$ reaction versus p laboratory angle obtained at average π detection angles of $\theta_\pi = 67^\circ$, 82° , 97° , and 112° , and average photon energies $E_\gamma = 300$ and 340 MeV. The E_γ , θ_π , ϕ_π , θ_p , and ϕ_p bins are listed in Table I. The results are integrated over the E_π and E_p acceptances of the detectors.

arise mostly from two-step processes either involving charge exchange or hadronic scattering, or combinations of both. Since the initial interactions are predominantly quasifree π production reactions and the second stage interactions tend to be forward peaked, the (γ, π^-p) results tend to mirror the quasifree results. This conclusion was supported by calculations based on the phenomenological Valencia model [34], which reproduced the shapes of the distributions and gave approximately the correct cross section magnitudes. The Valencia model is not appropriate for nuclei lighter than ${}^6\text{Li}$, but the close similarity with ${}^{12}\text{C}(\gamma, \pi^+p){}^{11}\text{Be}$ leads us to conclude that the ${}^4\text{He}(\gamma, \pi^+p)nnn$ reaction most likely arises mainly from two-step processes.

An alternative explanation has been proposed to explain part of the ${}^{12}\text{C}(\gamma, \pi^+p){}^{11}\text{Be}$ data by Fix *et al.* [15]. These authors have developed a model to describe photon interactions with preexisting Δ^{++} particles in nuclei and suggest that a fraction of the ${}^{12}\text{C}(\gamma, \pi^+p){}^{11}\text{Be}$ cross section arises from that process. However, it was found that the number of

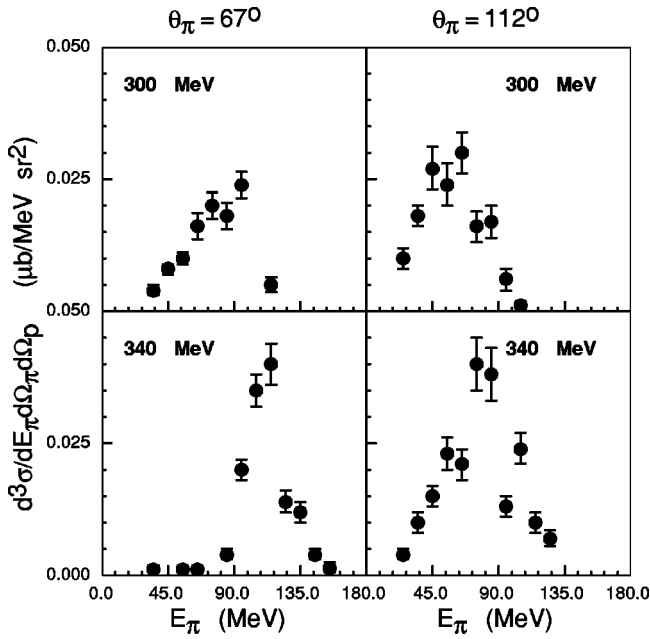


FIG. 12. Differential cross sections for the ${}^4\text{He}(\gamma, \pi^+ p)nnn$ reaction versus π^+ kinetic energy. The θ_π and θ_p bins are 10° and 15° wide, respectively. The ϕ_π and ϕ_p bins are listed in Table I. The results are integrated over the E_p acceptance of the detector.

Δ 's of all types per nucleon required to fit the data (7%) is considerably larger than that predicted for finite nuclei (generally less than 4%) [15]. Although, a similar analysis has not been carried out for the ${}^4\text{He}(\gamma, \pi^+ p)nnn$ reaction, it is evident from the fact that the cross sections per nucleon are of a similar magnitude to those for the ${}^{12}\text{C}(\gamma, \pi^+ p){}^{11}\text{Be}$ reaction that such an analysis would yield unexpectedly high probabilities for finding Δ^{++} particles in ${}^4\text{He}$.

Despite the above considerations, an explanation of the ${}^4\text{He}(\gamma, \pi^+ p)nnn$ and ${}^{12}\text{C}(\gamma, \pi^+ p){}^{11}\text{Be}$ results in terms of direct interactions with preexisting Δ^{++} particles cannot simply be ruled out. In their analysis, Fix *et al.* used a mean value for the Δ^{++} magnetic moment of $\mu_{\Delta^{++}} = -2.3$ nm. However, they point out that if they were to use $\mu_{\Delta^{++}} = 4.3$ nm, which may be more realistic, then typical results for the number of preexisting Δ^{++} particles of all types per nucleon of $\sim 1.7\%$ would be obtained. On this point, it is interesting to note that the θ_π distributions of π^+ particles deduced by inspection of Figs. 11 and 12 are rather flat. If these are compared to the θ_π distribution calculations presented in Ref. [15], they tend to support a high positive value

for $\mu_{\Delta^{++}}$, and a more realistic number of pre-existing Δ particles in ${}^4\text{He}$. Although two-step processes are the most likely explanation of the ${}^4\text{He}(\gamma, \pi^+ p)nnn$ results, an explanation in terms of direct interactions with preexisting Δ^{++} particles should be investigated further.

CONCLUSION

Data of good statistical accuracy have been obtained for the ${}^4\text{He}(\gamma, \pi^+ n){}^3\text{H}$ and ${}^4\text{He}(\gamma, \pi^+ p)nnn$ reactions over a wide range of E_γ , θ_π and θ_N using large solid-angle plastic scintillator arrays in coincidence with unpolarized and linearly polarized tagged photons. The missing energy resolution obtained was sufficiently good to indicate that events observed from the ${}^4\text{He}(\gamma, \pi^+ n){}^3\text{H}$ and ${}^4\text{He}(\gamma, \pi^+ p)nnn$ reactions arose predominantly from removing a $1s$ proton leading to the ${}^3\text{H}$ ground state and population of the $3n$ continuum, respectively. A comparison of the ${}^4\text{He}(\gamma, \pi^+ n){}^3\text{H}$ angular distributions and π kinetic energy spectra to calculated cross sections made using harmonic oscillator wave functions suggests that the use of such wave functions is sufficient to describe $(\gamma, \pi N)$ quasifree reactions, in contrast to the conclusions of Hicks *et al.* [14]. A comparison of the ${}^4\text{He}(\gamma, \pi^+ n){}^3\text{H}$ and ${}^{12}\text{C}(\gamma, \pi^+ n){}^{11}\text{B}$ data to calculated cross sections including crude FSI corrections, show trends in the data which could possibly be related to $\Delta(1232)$ -medium effects. This work and our previous paper [12] provide a substantial amount of new data on quasifree π production, which hopefully will provide a basis for future tests of theoretical models of $\Delta(1232)$ -medium effects leading to a more quantitative understanding of the phenomenon. The ${}^4\text{He}(\gamma, \pi^+ p)nnn$ data most likely arise from two-step processes, although an interpretation in terms of direct photon interactions with preexisting Δ^{++} particles is not ruled out and should be investigated further.

ACKNOWLEDGMENTS

This work was supported by grants from the U.K. EPSRC, the British Council, the DFG (Grant No. Mu705/3), BMFT (Grant No. 06Tü 656), DAAD (Grant No. 313-ARC-VI-92/118), the EC [Grant No. SCI.0910C(JR)] and NATO (Grant Nos. CRG 920171, CRG 970268). The authors thank the Institut für Kernphysik of the University of Mainz for the use of its facilities and assistance during the experiment. Five of us (J.F.A., J.A.M., D.P.W., S.F., and C.J.Y.P.) would like to thank EPSRC for support.

- [1] G. Mao, L. Neise, H. Stöker, and W. Greiner, Phys. Rev. C **59**, 1674 (1999).
- [2] M.-Th. Hütt, A. I. L'vov, A. I. Milstein, and M. Schumacher, Phys. Rep. **323**, 457 (2000).
- [3] L. Van Daele *et al.*, Phys. Rev. C **65**, 014613 (2001).
- [4] F. Sammarruca and E. J. Stephenson, Phys. Rev. C **64**, 034006 (2001).
- [5] L. D. Pham *et al.*, Phys. Rev. C **46**, 621 (1992).

- [6] T. Sato and T. Takaki, Nucl. Phys. **A562**, 673 (1993).
- [7] X. Li, L. E. Wright, and C. Bennhold, Phys. Rev. C **48**, 816 (1993).
- [8] M. Vanderhaeghen, Ph.D. thesis, University of Utrecht, The Netherlands, 1995.
- [9] M. MacCormick *et al.*, Phys. Rev. C **55**, 1033 (1997).
- [10] B. Krusche *et al.*, Phys. Rev. Lett. **86**, 4764 (2001).
- [11] J. A. MacKenzie *et al.*, Phys. Rev. C **54**, R6 (1996).

- [12] D. Branford *et al.*, Phys. Rev. C **61**, 014603 (1999).
[13] M. Liang *et al.*, Phys. Lett. B **411**, 244 (1997).
[14] K. Hicks *et al.*, Phys. Rev. C **61**, 054609 (2000).
[15] A. Fix *et al.*, Nucl. Phys. **A646**, 417 (1999).
[16] I. Anthony *et al.*, Nucl. Instrum. Methods Phys. Res. A **301**, 230 (1991).
[17] S. J. Hall *et al.*, Nucl. Instrum. Methods Phys. Res. A **368**, 698 (1996).
[18] D. Lohmann *et al.*, Nucl. Instrum. Methods Phys. Res. A **343**, 494 (1994).
[19] S. Oberkirsch *et al.*, Nucl. Instrum. Methods Phys. Res. A **418**, 507 (1998).
[20] I. J. D. MacGregor *et al.*, Nucl. Instrum. Methods Phys. Res. A **382**, 479 (1996).
[21] P. Grabmayr *et al.*, Nucl. Instrum. Methods Phys. Res. A **402**, 85 (1998).
[22] J. R. M. Annand and B. Oussena, Nucl. Instrum. Methods Phys. Res. A **330**, 220 (1993); J. R. M. Annand, I. Anthony, and B. Oussena, *ibid.* **368**, 385 (1996).
[23] J. A. Mackenzie, Ph.D. thesis, Edinburgh University, 1995.
[24] J. F. Arneil, Ph.D. thesis, Edinburgh University, 1998.
[25] I. Blomqvist and J. M. Laget, Nucl. Phys. **A280**, 405 (1977).
[26] C. Betourne *et al.*, Phys. Rev. **172**, 1343 (1968).
[27] F. X. Lee and L. E. Wright, calculations carried out specifically for inclusion in this paper, 1998.
[28] J. M. Laget, Nucl. Phys. **A481**, 765 (1987).
[29] R. M. Davidson, N. C. Mukhopadhyay, and R. S. Wittman, Phys. Rev. Lett. **56**, 804 (1986).
[30] V. R. Pandharipande, I. Sick, and P. K. A. de Witt Huberts, Rev. Mod. Phys. **69**, 981 (1997).
[31] S. Wunderlich and F. A. Natter, Tübingen Internal Report 1/97, 1997 (unpublished).
[32] A. Kraus *et al.*, Phys. Rev. Lett. **79**, 3834 (1997).
[33] H-P. Krahn, Ph.D. thesis, Universität Mainz, 1996; R. Beck *et al.*, Phys. Rev. Lett. **78**, 606 (1997); R. Beck *et al.*, Phys. Rev. C **61**, 035204 (2000).
[34] R. Carrasco and E. Oset, Nucl. Phys. **A536**, 445 (1992); R. Carrasco, E. Oset, and L. L. Salcedo, *ibid.* **A541**, 585 (1992); R. Carrasco, M. J. Vicente Vacas, and E. Oset, *ibid.* **A570**, 701 (1994).